Time-of-day-dependent variation of the human liver transcriptome and metabolome is disrupted in MASLD

Manuel Johanns, Joel T Haas, Violetta Raverdy, Jimmy Vandel, Julie Chevalier-Dubois, Loic Guille, Bruno Derudas, Benjamin Legendre, Robert Caiazzo, Helene Verkindt, et al.

Time-of-day-dependent variation of the human liver transcriptome and metabolome is disrupted in MASLD

Manuel Johanns[1], Joel T. Haas[1], Violetta Raverdy[2], Jimmy Vandel[1], Julie Chevalier-Dubois[1], Loic Guille[1], Bruno Derudas[1], Benjamin Legendre[2], Robert Caiazzo[2], Helene Verkindt[2], Viviane Gnemmi[3], Emmanuelle Leteurtre[3], Mehdi Derhourhi[4], Amélie Bonnefond[4,5], Philippe Froguel[4,5], Jérôme Eeckhoute[1], Guillaume Lassailly[6], Philippe Mathurin[6], François Pattou[2,$], Bart Staels[1,$], Philippe Lefebvre[1,$,*]

[1] Univ. Lille, Inserm, CHU Lille, Institut Pasteur de Lille, UMR1011-EGID, F-59000 Lille, France.
[2] Univ. Lille, Inserm, CHU Lille, Institut Pasteur de Lille, UMR1190-EGID, F-59000 Lille, France.
[3] Univ. Lille, Inserm, CHU Lille, UMR 1172, Lille, France
[4] Univ. Lille, Inserm, CHU Lille, Institut Pasteur de Lille, UMR 1283/8199-EGID, F-59000 Lille, France.
[5] Department of Metabolism, Imperial College London; London, United Kingdom
[6] Univ. Lille, Inserm, CHU Lille, UMR 995-LIRIC, Lille, France

[$] These authors contributed equally to this work.

* Corresponding author:
Philippe Lefebvre
Inserm UMR1011, Bldg J&K
Faculté de Médecine Henri Warembourg, Pôle Recherche
Blvd du Prof Leclerc
59000, Lille, France
philippe-claude.lefebvre@inserm.fr
Tel +33.3.20974220

Keywords: Liver homeostasis/cohort/daytime rhythmicity /gene expression/metabolomic

Short title: Time-of-day-dependent rhythmicity in MASLD

Electronic word count: Abstract=222, main text=6,984

Number of figures and tables: 7/1

Use of AI in writing: none

Conflicts of interest: none

Financial disclosure: Funding sources were neither involved in the conduct of the research nor in the preparation of the article. They had no role in study design, in data collection, analysis and interpretation; in the writing of the report; and in the decision to submit the article for publication

Author's contributions: Conceptualization: MJ, JTH, JV, FP, BS, PL; Software: MJ, JTH, JV, MD; Validation: MJ, JTH, JV, BD, VR, JE, BS, PL; Formal analysis: MJ, JTH, JV, JE, PL; Investigation: MJ, JTH, JV, BD, MD, AB; Resources: AB, PF, FP, BS, PL; Data curation: MJ, JTH, JV, BD, MD, VR, PL; Writing: MJ, JTH, JV, BS, PL; Visualization: MJ, JTH, JV, PL; Supervision: BS, PL; Project administration: BS, PL ; Funding acquisition: FP, BS, PL.

ABBREVIATIONS

ANOVA	Analysis of variance
cAMP	Cyclic adenosine monophosphate
CCGs	Core clock genes
CRN	Clinical research network
DiHOME	Dihydroxy-9-octadecenoic acid
GO	Gene ontology
GPC	Glycerophosphocholine
HFD	High fat diet
HODE	Hydroxyoctadecadienoic acid
KEGG	Kyoto encyclopedia of genes and genomes
LPA	Lysophosphatidic acid
MASLD	Metabolic dysfunction-associated steatotic liver disease
MASH	Metabolic dysfunction-associated steatohepatitis
PA	Phosphatidic acid
PNPLA3	Patatin-like phospholipase domain–containing protein 3
PPARγ	Peroxisome proliferator-activated receptor gamma
PUFAs	Polyunsaturated fatty acids
TDG	Time-of-day-dependent genes
TDM	Time-of-day-dependent metabolites
TGFβ	Transforming growth factor beta
TLR	Toll-like receptor
TNFα	Tumor necrosis factor-alpha
TTFLs	Transcriptional-translational feedback loops

ABSTRACT

Background and aims: Liver homeostasis is ensured in part by time-of-day-dependent processes, many of them being paced by the molecular circadian clock. Liver functions are compromised in metabolic dysfunction-associated steatotic liver (MASL) and metabolic dysfunction-associated steatohepatitis (MASH), and clock disruption increases susceptibility to metabolic dysfunction-associated steatotic liver disease (MASLD) progression in rodent models. We therefore investigated whether time-of-day-dependent transcriptome and metabolome are significantly altered in human steatotic and MASH livers.

Methods: Liver biopsies, collected within an 8 hour-window from a carefully phenotyped cohort of 290 patients and histologically diagnosed to be either normal, steatotic or MASH hepatic tissues, were analyzed by RNA sequencing and unbiased metabolomic approaches. Time-of-day-dependent gene expression patterns and metabolomes were identified and compared between histologically normal, steatotic and MASH livers.

Results: We provide here a first-of-its-kind report of a daytime-resolved human liver transcriptome-metabolome and associated alterations in MASLD. Transcriptomic analysis showed a robustness of core molecular clock components in steatotic and MASH livers. It also revealed stage-specific, time-of-day-dependent alterations of hundreds of transcripts involved in cell-to-cell communication, intra-cellular signaling and metabolism. Similarly, rhythmic amino acid and lipid metabolomes were affected in pathological livers. Both TNFα and PPARγ signaling were predicted as important contributors to altered rhythmicity.

Conclusion: MASLD progression to MASH perturbs time-of-day-dependent processes in human livers, while the differential expression of core molecular clock components is maintained.

Impact and implications: This work characterizes the rhythmic patterns of the transcriptome and metabolome in human liver. Using a cohort of in-depth phenotyped patients (n=290) with known biopsy collection time-of-day, we show that time-of-day variations observed in histologically normal livers are gradually perturbed in liver steatosis and metabolically-associated steatohepatitis. Importantly, these observations, albeit obtained on a restricted time window, bring further support to preclinical studies evidencing alterations of rhythmic patterns in diseased livers. On a practical side, this study calls for considering time-of-the-day as a critical biological variable which may significantly affect data interpretation in animal and human studies of liver diseases.

Graphical abstract:

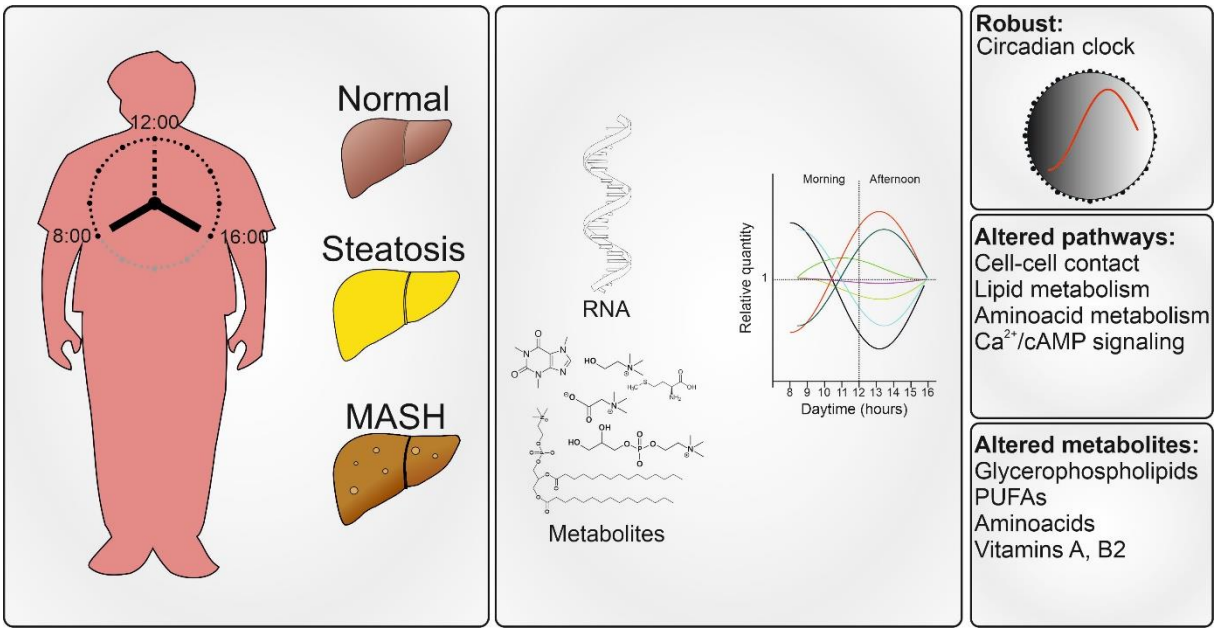

INTRODUCTION

Normal tissue homeostasis requires a precisely timed expression of genes and proteins around the clock and its alignment with cycles of light/dark exposure, feeding periods and physical activity. The central clock, located in the suprachiasmatic nucleus, is light-entrained and connects with peripheral tissues to synchronize clock oscillators in these tissues. However, peripheral tissue clocks can operate autonomously, *i.e.* independently of the central hypothalamic clock. For example, the major *Zeitgeber* ("time giver") setting the liver clock is food intake/nutrient availability rather than daylight [1, 2]. Studies in nocturnal rodents of molecular mechanisms controlling these circadian regulations generated a global picture defining an universal molecular clock machinery [3]. This cell-autonomous circadian core clock is made of 2 autoregulatory loops comprising 14 transcription factors, encoded by so-called core clock genes (CCGs). Heterodimeric BMAL1 (*ARNTL*) and CLOCK (or NPAS2) transcriptional activators and PER and CRY transcriptional repressors, along with the nuclear receptors RORs, REV-ERBα and β constitute interlocked transcriptional-translational feedback loops (TTFLs). These TTFLs define a cell-autonomous clock machinery which controls clock output genes [4], in turn regulating multiple cellular functions [3].

Because most of primates (including humans) are diurnal, there are likely important differences from rodents in circadian regulation that have yet to be explored. A limited number of human time-of-day-resolved transcriptomes is available, especially for internal organs. Transcriptomes from whole blood [5, 6], peripheral blood mononuclear cells [7], skin [8], subcutaneous white adipose tissue [9, 10], heart montaigne [11]or skeletal muscle [12-14]were analyzed for a relatively low number of subjects (n<30). A gene expression study in subcutaneous white adipose tissue and skin from 625 healthy volunteers allowed the identification of time-of-day-regulated genes strongly enriched in CCGs [15].

Circadian rhythm dyssynchrony is observed in, and likely causative of, various diseases such as obesity and its complications like metabolic dysfunction-associated steatotic liver disease (MASLD), formerly known as non-alcoholic fatty liver disease (NAFLD). MASLD is a spectrum of liver conditions characterized by hepatic steatosis which combines, upon time, with varying degrees of necroinflammation and excluding excessive alcohol consumption [16]. Its more severe, yet generally asymptomatic form, called metabolic dysfunction-associated steatohepatitis (MASH; formerly known as NASH, non-alcoholic steatohepatitis), may evolve

towards liver fibrosis, cirrhosis and hepatocellular carcinoma Large-scale MASLD patient cohort studies reported differences in gene expression between disease stages without time-of-day information [17-20]. While hepatic metabolomes and transcriptomes are deregulated in rodent models of MASH and fibrosis [21, 22], whether this occurs similarly in human MASLD remains unknown. A 24 hour-circadian transcriptome atlas of 64 tissues from healthy baboons identified only a small set of robustly cycling genes in liver, surprisingly not including CCGs [23]. Rhythmic gene expression patterns were inferred from the analysis of tissues collected *post mortem* from 600 human donors. Relatively few genes (n=648), including only a few CCGs, exhibited predicted time-of-day-dependent expression [24]. Thus, both ethical and technical hurdles hinder the thorough investigation of time-of-day-dependent processes in healthy human liver and the deregulation thereof in MASLD. Importantly, this conclusion extends to the hepatic metabolome, which is clock-controlled and disturbed in various liver dysfunction models [22, 25-28]. Disturbances in the hepatic chronometabolome observed in rodent MASLD models have not been reported for humans so far [29].

Considering these knowledge gaps, we asked whether the hepatic time-of-day-dependent transcriptome and metabolome are affected during MASLD progression. We leveraged a large cohort of morbidly obese patients undergoing bariatric surgery from whom liver biopsies were taken peri-operatively (HUL cohort, [18]). Hepatic transcriptomes and metabolomes were obtained from a sub-cohort of 290 patients whose biopsies were histologically identified as either normal, steatotic, or MASH livers and for which the exact biopsy time-of-day was known (Figure 1A). In an original approach integrating multiple statistical tests, we provide the first-ever robust analysis of time-of-day-dependent gene expression and tissue metabolite abundance in human liver, as well as changes associated with the different stages of MASLD.

MATERIALS and METHODS

Liver biopsies from the HUL cohort

The Hôpital Universitaire de Lille (HUL) cohort, also known as the Biological Atlas of Severe Obesity (ABOS) cohort was established as from 2006 by the University Hospital of Lille, France (ClinicialTrials.gov: NCT01129297) from severely and morbidly obese patients visiting the Obesity Surgery Department. The study protocol conforms to the ethical guidelines of the 1975 Declaration of Helsinki. All patients of the cohort fulfilled criteria for, and were willing to undergo, bariatric weight-loss surgery (for details, see [18]). Written informed consent was obtained from each patient included in the study. The protocol required that patients were fasting from midnight to surgery time. During the surgical procedure, wedge biopsies were taken from the liver to be immediately snap-frozen and the exact time of the biopsy was noted. A total of > 1,500 patients are currently included in the HUL cohort, amongst whom 319 were selected to build a sub-cohort with complete clinical, biometric parameters and a robust histological MASLD classification of quality-controlled biopsies eliminating all intermediary MASLD stages (see [18] and Figure 1B for more details). Both transcriptomes and metabolomes were obtained for these 319 patients with biopsy mass >100mg. Out of these, 290 had known biopsy time-of-day, ranging from 8am to 4pm, and were included in this study. Main clinical and histological characteristics are indicated in Table 1. Patient clinical data shown in Table 1 were analyzed using the package “gtsummary” (v1.5.0).

Total RNA sequencing and data processing

A detailed procedure can be found in the Supplemental Information file.

Liver metabolomics by LC-MS

All tissue samples were flash frozen and maintained at –80°C until processing. Sample preparation was carried out as described previously [30] at Metabolon, Inc. (Morrisville, NC, USA). A detailed procedure can be found in the Supplemental Information file.

Bioinformatic analysis

Bulk RNAseq: All analyses were carried out using RStudio (v1.4.1106) with R (v4.1.0). Data processing for differential expression as a function of time-of-day can be found in the Supplemental Information file.

Single cell RNAseq: All analysis has been made under R (v 4.2.0). A detailed procedure for data extraction and processing can be found in the Supplemental Information file.

Enrichment analysis

Time-dependent gene lists were analyzed for enrichment of Kyoto Encyclopedia of Genes and Genomes (KEGG) pathways and gene ontology (GO) biological process terms using Metascape 3.5 [31] with default settings (https://metascape.org/). A detailed procedure for data processing can be found in the Supplemental Information file.

Data visualization and illustrations

Graphs were generated as *.svg files using R packages mentioned above. Data were imported in CorelDraw2020 to assemble figures. Drawings in Figure 1A are from Renée Gordon, Victovoi, and Mikael Häggström, M.D. and were made available to the public domain via Wikimedia Commons with no restriction of use. Bubbleplots were generated in R studio using the ggplot2, plotly, reshape2, rcpp, and tidyverse packages as described in [32].

RESULTS

Time-of-day is a major factor affecting gene expression in human liver

Human liver biopsies were collected from patients with obesity and undergoing bariatric surgery, for which the exact daytime of the liver biopsy was recorded (Figure 1A). Key clinical parameters of the 290 patients are summarized in Table 1. Based on histological features of liver biopsies (steatosis, hepatocyte ballooning, lobular inflammation), patients were grouped according to MASLD stages and labelled as histologically normal (HN), steatotic or MASH liver following the decision tree shown in Figure 1B. The proportion of men in this cohort increased with MASLD severity, rising from 16% (HN) to 38% (MASH) with an average Clinical Research Network (CRN) NAS score rising from 0 to 5, respectively. Since sex is an important biological variable in this context [18], this was considered during further analysis (see below). Patients in the steatosis and MASH groups were slightly older than those in the HN group, and expectedly had also higher insulin resistance on average.

The source of variation in gene expression levels was estimated by a multivariate analysis of variance (ANOVA) (Figure 1C). The F-ratio (ratio of the between-group variance to the within-group variance) not only confirmed sex and group (*i.e.* MASLD stage) as the main sources of variation as previously reported [18], but very interestingly identified biopsy time (AM *vs.* PM) as the third most significant source of variation (Figure 1C). Age had only a minor contribution to signal variation. The distribution of biopsy times (Figure 1D) revealed a daytime window of about 8 hours. Biopsies were predominantly (>60%) taken in the morning with a first peak around 9:30 AM and a second, lower peak around 2:30 PM, due to the logistical schedule of surgical interventions. There was, however, no significant difference in biopsy time distribution between histological groups (Table 1). Since exclusion of biopsies collected between 11am and 1pm did not modify the outcomes of preliminary statistical analysis, the “AM“ subgroup was defined as biopsies taken before noon (12:00), the “PM” subgroup as biopsies taken after noon.

Gene expression profiles were thus compared between morning (AM) *vs.* afternoon (PM) samples. Differentially expressed genes were identified using DEseq2 independent of the MASLD status but correcting for sex. Transcript counts for 1,660 genes were significantly

different (Benjamini-Hochberg adjusted p-value <0.05) between AM or PM biopsies (Figure 1E). Among the 100 top hits were most of the CCGs (*PER3, ARNTL/BMAL1, NPAS2, NR1D1, NR1D2, PER2, CRY1, PER1*), clock-related genes (*CIART*, *DBP, NFIL3)* (Figure 1E) as well as circadian-regulated genes involved in lipid metabolism (*PPARD*, *LIPG, LPIN2…)*. Because patients were fasting from midnight irrespective of surgery time, genes implicated in hepatic gluconeogenesis (*G6PC, PCK1, SGK2…)* were, as expected, higher expressed in PM samples (Figure 1E and Supp. Table 1). Opposite to nocturnal rodents, genes from the negative limb of the clock displayed lower expression in the afternoon (*PER3, NR1D1, NR1D2, CIART…*), whereas genes from the positive clock limb were higher expressed in the afternoon (*ARNTL/BMAL1, NPAS2…*)(Figure 1E). Globally, genes displaying AM *vs.* PM differential expression were significantly enriched for the KEGG pathways "circadian rhythm", "PPAR signaling pathway", carbohydrate and lipid metabolic pathways, as well as cellular architecture and communication, among others (Figure 1F).

Thus an 8-hour time frame allowed the detection of significant changes in time-of-day-dependent liver gene expression, with a large proportion of transcripts functionally related to circadian rhythmicity.

Time-dependent genes vary between MASLD stages

We next examined whether time-of-day-dependent distributions of gene expression would differ between the histological states "HN", "steatosis" and "MASH". In order to achieve statistical power and obtain robust and exhaustive lists of time-dependent gene expression over the available daytime window, we used 3 complementary statistical methods analyzing different aspects of gene expression distribution (differential expression, partial Spearman correlation, Kolmogorov-Smirnov test), the results of which were agglomerated by a Fisher test to yield a combined p-value for each gene (Figure 2A-C and Supp. Figures 1 and 2). The 3 types of analyses are graphically exemplified for the core clock gene *ARNTL/BMAL1* (Figure 2A-C) which served as positive control to validate our approach, as it is among the most highly time-dependent genes regardless of the histological group. First DEseq2, which relies on a negative binomial distribution of gene expression, was used to identify differential gene expression between 2 conditions (AM *vs.* PM as in Figure 1) (Figure 2A). Second, partial

Spearman correlation was computed between *ARNTL* gene expression and daytime (Figure 2B). Both approaches integrated sex as a confounding factor. Third, the Kolmogorov-Smirnov test was employed to determine whether AM and PM *ARNTL* expression distribution followed a similar law and thus were similar in shape (Figure 2C). Finally, the Fisher combined probability test or "Fisher's method" was used as a meta-analysis method for p-value combination: individual raw p-values resulting from each statistical test were agglomerated into a single p-value per group (Figure 2D). The detected expression profile of *ARNTL*, of other CCGs (Supp. Figure 1) and of all other transcripts (Supp. Figure 2), clearly confirmed that the available time window was sufficient for robust time-of-day analysis of gene expression. A total of 1,427 genes with an absolute fold change greater than 1.2 (AM *vs.* PM) (FDR <0.01) was identified (Figure 2E). The vast majority of these time-dependent genes (TDGs) were strikingly distinct when comparing the 3 patient groups. Less than 10% (132 genes) were indeed common to all 3 groups ("common TDGs") (Figure 2E) and notably included most CCGs (*ARNTL, NR1D1/2, NPAS2, CRY1, PER1/2/3, DBP, CIART*)(Supp. Table 1). TDG repartition outside of this core set was strongly unequal between groups, with ≈50% (558) of non-shared TDGs found in HN, ≈35% (392) in steatotic and less than 15% (177) in MASH livers. Along the same line, we found that AM to PM fold changes of common TDGs were, on average, decreased in steatotic and even more in MASH livers when compared to HN livers (Figure 2F). These differences are illustrated for a selection of TDGs with AM-PM differences either decreasing (*PCAT18, ARMC4, SIK1B*) or increasing in MASH (*CYP4Z1, RHOBTB1, PPIAP71*)(Figure 3A,B).

Common TDGs were collectively enriched for KEGG terms like "circadian rhythms" as expected from the content in transcripts coding for CCGs, and for metabolic regulatory pathways like the PPAR and FoxO pathways (Figure 4, Supp. Figure 3), illustrated by genes such as *S1PR1, G6PC1, PCK1, SGK2, FASN, AQP7* and *PPARD*. TDGs unique to the HN group were also enriched, albeit to a lesser extent, for pathways linked to circadian rhythm (notably including *CLOCK*) as well as to fatty acid and amino acid~~s~~ metabolism. The most highly represented pathway was "gap junctions" (Figure 4A, Supp. Figure 3), characterized by genes such as *PDGFB, MAP2K1* and transcripts encoding for tubulins *TUBA1C/8, TUBB, TUBB1/2B* (Supp. Table 1), suggesting that epithelial barrier integrity/permeability homeostasis, which is known to be disturbed in MASLD [33], requires an oscillating expression of these genes in

healthy conditions. Genes unique to the steatosis group (Supp. Table 1) were mostly linked to metabolism of lipids and fatty acids (*DGKG, PLA2G4B/5, LPIN2/3, ETNK2, ETNPPL, PLPP4, FADS1/2, CYP2C8, GDPD1, SCD*) and also to metabolism of peptides and amino acids (*DNMT3B, GCLM, SDS, PSAT1, GNMT, ALDOC, GPT2, CSAD, UPB1*)(Figure 4A, Supp. Figure 3). Lastly, TDGs specific to the MASH group (Supp. Table 1) were highly enriched for signaling by calcium, cAMP or neurotransmitters (*ADRB2, DRD1, GRM1, NTRK1, NTSR1, P2RX7, RYR2, CACNA1H, SSTR5, TBXA2R, FFAR2, SUCNR1)* as well as for lipolysis (*ADRB2, IRS1, PNPLA2*)(Figure 4, Supp. Figure 3). The temporal pattern of gene expression in homeostatic conditions is thus strongly affected by the disease state and indicative of compromised cellular communication and metabolic pathways.

Inferring upstream regulatory cues or altered biological processes may be achieved by comparing differentially expressed gene lists to consensus gene expression patterns induced by a given perturbagen (Figure 4B-D). Speed2 (Signaling Pathway Enrichment using Experimental Datasets [34]) analysis allows probing gene lists against ranked gene signatures for 16 signaling pathways, with the aim of identifying upstream signaling mediators. Ranked signatures suggested that cues in homeostatic (HN) conditions could be TGFβ, TNFα, oxidative stress, TLR and estrogen (Figure 4B). In steatosis and MASH conditions, this pattern shifted towards a more limited signaling pathway panel with similar statistical significance, which included either TLR and VEGF (steatosis) or TNFα and TLR (MASH)(Figure 4C and 4D respectively). Although causative links cannot be proven, this data could reflect a loss of physiological rhythmic function(s) in steatotic and MASH livers, which in turn gain rhythmic functions associated to pathogenic immune and proliferative stimuli and responses.

MASLD stages correlates with time-of-day changes in liver metabolites

Our results suggested that metabolic pathways are altered in a time-of-day-dependent manner as MASLD progresses, with an enrichment in amino acid- and lipid metabolism-regulating genes (Supp. Figure 3). Therefore, an unbiased tissue metabolomic study by LC-MS was performed on the same 290 liver samples. Similar to the gene expression analysis, a global approach was initially employed to evaluate overall time-of-day dependence of tissue metabolite levels regardless of the MASLD status. This global analysis identified ≈220 metabolites whose amounts were significantly different in AM and PM biopsies (DEseq2

corrected for sex, FDR<0.1) (Figure 5A, Supp. Table 2). Visual inspection of the volcano plot highlighted intermediates of lipid β-oxidation (carnitine derivatives), amino acids (kynurenate, oxo-arginine…) as differentially detected in AM *vs.* PM livers (Figure 5A). It also confirmed the more marked fasting status of "PM" patients exhibiting an increased hepatic content in 3-hydroxybutyrate (BHBA). A biological term enrichment analysis confirmed that the majority of the identified metabolites belonged to amino acid, lipid and fatty acid metabolic pathways (Figure 5B).

To highlight a possible time-of-day differential representation of metabolites between MASLD groups, we again combined the 3 statistical approaches as described for gene expression analysis (DEseq2, Spearman correlation, Kolmogorov-Smirnov test) followed by Fisher's agglomeration for a robust identification of time-dependent metabolites (TDMs) (Figure 5C). A total of 251 TDMs were identified using this method (combined FDR<0.1), out of which only 14 (6%) were common to all 3 MASLD groups (Figure 6A, 6B). These common TDMs included amino acids such as proline and threonine, several fatty acids and the ketone body component β-hydroxybutyrate (Figure 6B and Supp. Figure 4A-F). KEGG metabolic pathway enrichment analysis revealed that these common TDMs were most significantly associated to metabolism of amino acids (arginine, proline, threonine)(Figure 6B and Supp. Figure 4A-C). In agreement with the identification of the PPAR pathway based on gene expression patterns (Figure 4) and the detection of 3-hydroxybutyrate (Supp. Figure 4D), synthesis of ketone bodies was also identified as a relevant term (Figure 6B),

Among the 197 stage-specific TDMs, 31% were specific to HN, 47% to steatosis and 20% to MASH (Figure 6A and Supp. Table 2). TDMs specific to HN livers, and thus lost at the steatosis and MASH stages, were mainly associated to metabolism of sphingolipids (Figure 6C and Supp. Table 2) such as CDP-choline and sphinganine (Supp. Figure 4G, H). Glycerophosphoethanolamines, glycerophosphocholines as well as derivatives of cholesterol, amino acids and pyrimidine were also identified as time-dependent in normal livers (Supp. Table 2 and Supp. Figure 4I-L).

A similar enrichment analysis identified amino acid metabolic pathways (branched-chain, sulfur-containing, arginine, taurine) (Figure 6D, Supp. Figure 5A, B and Supp. Table 2) as time-dependent in steatotic livers. Visual inspection of steatosis TDMs also identified a carnitine precursor (N6,N6,N6 trimethyl-lysine, Supp Figure 5C) and derivatives (Supp. Table

2 and Supp. Figure 5D, E) which could reflect an altered fatty acid oxidation activity. Finally, MASH-specific TDMs were enriched mainly for vitamin, glycan and glycosylphosphatidylinositol (GPI) metabolic intermediates (Figure 6E, Supp. Figure 5 and Supp. Table 2).

Taken together, these analyses highlight the disruption during MASLD progression of time-of-day-dependent bioactive phospholipid metabolism and of amino acid biotransformation pathways. Intriguingly, PPARγ ligands of the linoleic acid class (9,10 DiHOME [35] and 9- and 13-HODE [36]) displayed a differential abundance in AM *vs.* PM steatotic and MASH livers, with estimated concentrations in the 10-100µM range which are sufficient to activate PPARγ (Supp. Figure 5F, J).

Integrative analysis of time-dependent genes and metabolites.

We next performed an integrative analysis of the transcriptomic and metabolomic data at the pathway level using the KEGG database. This analysis combined TDGs and TDMs specific to either HN or MASH stages and common TDGs and TDMs, irrespective of their relative time-of-day direction of change, to identify associated transcriptomic and metabolomic conditions operating in normal and MASH livers (Figure 7A). TDGs and TDMs characterizing the HN stage were enriched for metabolic pathways related to lipid and amino acid metabolism, while most of them were not detected at the MASH stage, or with a decreased significance [arginine (Arg) and proline (Pro) metabolism, glycerophospholipid metabolism]. Linoleic metabolism was associated to the MASH stage (Figure 7B, C). HN-or MASH-enriched pathways (glycerophospholipid and linoleic pathways, respectively) were further detailed for daytime variation of associated TDGs and TDMs. The glycerophospholipid pathway was characterized by an increased abundance in AM livers of 3 out of 4 detected diacylglycerol (DAG) species specifically at the HN stage. Glycerophosphocholine (GPC) intermediates (CDP-choline, GPC) displayed stage-specific time-of-day variations that were not correlated to the occurrence of glycerophospholipid species (X-GPC) (Figure 7D). Higher abundance of DAG species in the morning did not correlate with HN TDG expression changes in transcripts encoding enzymes involved in this metabolic pathway, with the exception of the patatin-like phospholipase domain–containing protein 3-encoding gene (*PNPLA3*). PNPLA3/adiponutrin has

acyltransferase activity, increasing the formation of phosphatidic acid (PA) from lysophosphatidic acid (LPA), which may lead to more DAG synthesis. It might also reflect PNPLA3 hydrolytic activity on triacylglycerol molecules, favoring DAG accumulation. Along the same line, we compiled TDG and TDM data related to linoleic acid metabolism (Figure 7E). The increased abundance of the PPARγ ligands 9- and 13-HODE in the afternoon at the MASH stage was mirrored by the gene expression of *ALOX15*, a dioxygenase catalyzing the synthesis of these 2 hydroxyoctadecadienoic acids which was higher in the morning. A similar lack of correlation was observed between 9,10-DiHOME hepatic content and the expression of the linoleic acid-converting *CYP2C8* at the steatosis stage. These results suggest that time-dependent metabolite variation in these pathways is delayed with respect to gene regulation, and/or controlled by post-transcriptional processes.

Of note, mapping of human transcript expression to liver cell types using a reference single cell RNAseq dataset [37] suggested that the identified enzymatic pathways may follow a cell-specific expression pattern. They appear as mainly restricted, but not limited to, hepatocytes. As an example, *ALOX15* is detected in dendritic cells, whereas *ALOX5* is also detected in monocytes, neutrophils and basophils (Supp. Figure 6). Therefore time-dependent metabolite variation may occur in either identical or distinct cell types, reflecting a functional compartmentalization. Yet these observations confirmed the presence of time-of day variation in hepatic gene expression and metabolome, and identified several new oscillating metabolites at the MASH stage (Figure 7 and Supp. Table 2).

DISCUSSION

Chronobiological studies require multiple replicates at 2h-intervals over a total period of 24 or even 48 hours, within a controlled environment including timed exposure to light and food. These conditions are not achievable in human studies, precluding the analysis of cyclic processes and particularly in internal organs [38]. While human circadian rhythms are appreciated by genome-wide association study studies and the phenotypic manifestation of disturbed cyclic processes such as sleep, light exposure and eating patterns [39], their study in healthy or pathological conditions is indeed hindered by ethical and technical constraints. Despite controlled experimental setup with regard to sleep behavior and food intake in previous studies [5-14], a limited number of samples of mostly healthy individuals were collected, thereby limiting data interpretation due to high inter-sample variability.

Here we reveal the first ever time-of-day-resolved human liver transcriptome with associated liver tissue metabolites using a 290-patient cohort. Although the available time window of liver biopsies was only about 8 hours, this temporal window was sufficient to robustly identify TDGs and TDMs. Time-dependency of genes and metabolites was distinct between histologically-defined MASLD groups. However, a small proportion of genes was identified as time-dependent in all three patient groups and included CCGs, indicating that the molecular lock is rather robust in pathological conditions. In contrast, the alignment of rhythmic biological processes such as intercellular communication (gap junctions) and metabolic regulations is disrupted upon MASLD progression. Interestingly, none of the detected TDGs in MASH patients belonged to the human and mouse core set of MASH/fibrosis-associated genes [20], underlining the need for considering time as an important biological variable. Interestingly, the number of stage-specific TDGs (Figure 2E) decreases from the HN to the MASH stage, and concomitantly enriched pathways lessen (Supp. Figure 3), hinting at a loss of functional adaptability/(metabolic) flexibility. In high fat diet (HFD)-fed mice, transcripts gaining rhythmicity when compared to chow diet-fed mice are strongly enriched for glycerophospholid metabolism [22], similarly to steatotic patients (Supp. Figure 3), indicating convergent mechanisms for liver adaptation to dietary imbalance as often occurring in MASLD. At the cellular level, Ca^{2+} fluxes are submitted to ultradian variations and coupled to metabolic regulations [40], and mishandled intracellular Ca^{2+} stores in MASH can significantly impact parenchymal and non-parenchymal liver cellular functions [41]. A number

of genes encoding for Ca^{2+} channel components or involved in intracellular Ca^{2+} signaling (*PKD1L1*, *TRPC1 P2RX7*, *FFAR2*, *ADRB2*, *CACNA1H*, *GRM1*, *NTRK1*) exhibited differential AM *vs.* PM expression specifically in MASH livers. Thus, in addition to the lipid-induced dysfunctional ER Ca^{2+} transport [42], *de novo* oscillation of the calcium handling process accompanies progression to MASH. *CLOCK* gene deletion affected metabolite oscillations in mouse liver [25] and we detected a time-of-day differential expression of *CLOCK* exclusively in HN livers, which display a more diverse metabolic activity than MASH livers (Figure 7B). While hinting at a possible role of (the loss of) CLOCK, the examination of individual metabolites nevertheless showed little overlap between mouse CLOCK-dependent metabolites and HN-specific metabolites. This lack of clear concordance can be explained by species-specific mechanisms, distinct effects of gene deletion *vs.* loss of time-dependent expression and/or technical bias.

While examining the coherence between MASLD state-specific liver transcriptomes and metabolomes, we observed little correlation between enzyme-encoding genes and metabolite abundance. This disconnection is not unprecedented and was also observed in a highly standardized mouse study which minimizes the variability typically observed in human samples [22]. The narrow time window of our study may explain in part this lack of correlation as transcripts are likely to precede metabolite production, hence affecting our statistical approach for the PM sub-cohort. It may also indicate significant time-of-day-dependent translational control [43] as well as post-translational modifications regulating enzyme activity which are not captured by our analysis.

Finally, another point of convergence between our and mouse studies is the differential abundance of linoleic acid derivatives and PPARγ ligands 9,10--DiHOME, 9-HODE and 13-HODE in steatotic and MASH livers, respectively. The PPARγ-encoding gene *NR1C3/PPARG* itself did not display significant oscillatory expression in human liver, contrasting with HFD mouse livers [22]. Whether estimated released concentrations of these compounds are indeed sufficient to differentially activate human liver PPARγ, which is mostly expressed in endothelial cells, hepatocytes and macrophages (Supp. Figure 6) and have a causative role in hepatic transcriptional reprograming requires further in-depth investigation.

On the one hand, it is remarkable that many of the biological processes and pathways shown to be affected by MASLD in other studies, identified on the basis of changes in gene

expression or metabolite abundance levels regardless of time, also display altered time-dependent expression profiles in our study. On the other hand, we identified many novel potential links between genes with deregulated timed expression and MASLD pathogenesis, which were not previously considered by standard analyses. It is probably the combination of both types of deregulations that underlies the deeply disturbed liver functions once MASH is declared. Conversely, some of the changes detected when time-of-day information is absent or ignored may turn out to be artefacts, as time-of-day as a biological variable might not be equilibrated between groups.

Considering that the time-of-day dependence of transcript/protein/metabolite measurements was previously neglected or ignored in nearly all human MASLD studies, our findings here reveal a significant impact of time-of-day on many relevant pathogenic processes. As such, differences found between sample groups in cohort studies might reflect a previously under-appreciated bias in sampling time between groups. Further investigation is needed in this regard, particularly when studying human material. In any case, a new generality should be that sampling daytimes (or *Zeitgeber* times) must be carefully recorded and included in post-hoc analyses whenever possible.

Strengths and limitations of the study.

This study has both strengths and limitations. This first-of-its-kind study revealed time-of-day transcriptomic and metabolomic alterations in human livers as a function of the histologically-proven MASLD stage. It used a large cohort allowing both the selection of biopsies to adequately encompass healthy control, steatosis and MASH cases and robust statistical analysis. There is however a number of limitations, inherent to the observational nature of the study. The narrow time window for biopsies collection (8 hours) precludes the assessment of a 24h diurnal rhythmicity, hence of the integrity of the molecular clock. The unavoidable difference in fasting duration could also be a confounding factor.

Our bulk RNA sequencing approach allowed a full coverage of the transcriptome, but precluded the identification of liver cell types expressing TDGs. We thus calculated a cell specificity index of TDGs in human resident parenchymal (PC, hepatocytes) and non-parenchymal (NPC) $CD45^-$ cells. The tau (τ) index, calculated by a robust and simple method

to assess cell-type specificity, was used as a metrics [44]. Using a reference single cell-RNA sequencing dataset for human livers collected at unknown times [37], τ could be calculated for 584 transcripts out of the 1,481 identified TDGs (Supp. Table 1). Using this metric, only 51 genes displayed a cell type-restricted expression pattern in $CD45^-$ cells (τ>0.85), which was not limited to hepatocytes (Supp. Figure 7). The remaining 533 transcripts including CCGs could be mapped to 2 or more cell types. Of note, 15 out of the 51 cell-restricted transcripts were mostly expressed in dendritic or Kupffer cells (Supp. Figure 6).

Taken together, our bulk RNAseq approach detected a high number of TDGs than previous efforts, including many pathways never previously reported as being time-dependent. This resource will serve as an important basis for further investigations considering also the cell-type specificity in time-of-day gene expression variation in human MASLD.

ACKNOWLEGMENTS

This work was supported by ANR (RHU PreciNASH 16-RHUS-0006, EGID ANR-10-LABX-0046 and DeCodeNASH ANR-20-CE14-0034). MJ was supported by Wallonie-Bruxelles International (WBI, Belgium, ref. SUB/2020/479801) and from European Association for the Study of the Liver (EASL, Sheila Sherlock fellowship). JTH and AB hold a European Research Council (ERC) grant (StG, Metabo3DC, contract number 101042759; CoG, OpiO, contract number 101043671 respectively). PL's and BS's teams are supported by Fondation pour la Recherche Médicale (Equipes labellisées FRM EQU202203014645 and FRM EQU202203014650 respectively).

DATA AVAILABILITY

Further information and requests for resources and data sets should be directed to and will be fulfilled by the corresponding author. Data exploration of the HUL cohort is still ongoing and restrictions apply to clinical data availability.

Bibliography

Author names in bold designate shared co-first authorship.

[1] Li H, Zhang S, Zhang W, Chen S, Rabearivony A, Shi Y, et al. Endogenous circadian time genes expressions in the liver of mice under constant darkness. BMC Genomics 2020;21:224.

[2] Chaix A, Lin T, Le HD, Chang MW, Panda S. Time-Restricted Feeding Prevents Obesity and Metabolic Syndrome in Mice Lacking a Circadian Clock. Cell Metab 2019;29:303-319.

[3] Sato T, Sassone-Corsi P. Nutrition, metabolism, and epigenetics: pathways of circadian reprogramming. EMBO Rep 2022;23:e52412.

[4] Takahashi JS. Transcriptional architecture of the mammalian circadian clock. Nat Rev Genet 2017;18:164-179.

[5] **Archer SN, Laing EE**, Möller-Levet CS, van der Veen DR, Bucca G, Lazar AS, et al. Mistimed sleep disrupts circadian regulation of the human transcriptome. Proc Natl Acad Sci U S A 2014;111:E682-691.

[6] **Möller-Levet CS, Archer SN**, Bucca G, Laing EE, Slak A, Kabiljo R, et al. Effects of insufficient sleep on circadian rhythmicity and expression amplitude of the human blood transcriptome. Proc Natl Acad Sci U S A 2013;110:E1132-1141.

[7] Kervezee L, Cuesta M, Cermakian N, Boivin DB. The phase-shifting effect of bright light exposure on circadian rhythmicity in the human transcriptome. J Biol Rhythms 2019;34:84-97.

[8] Wu G, Ruben MD, Schmidt RE, Francey LJ, Smith DF, Anafi RC, et al. Population-level rhythms in human skin with implications for circadian medicine. Proc Natl Acad Sci U S A 2018;115:12313-12318.

[9] Christou S, Wehrens SMT, Isherwood C, Möller-Levet CS, Wu H, Revell VL, et al. Circadian regulation in human white adipose tissue revealed by transcriptome and metabolic network analysis. Sci Rep 2019;9:2641.

[10] Zhao L, Hutchison AT, Liu B, Wittert GA, Thompson CH, Nguyen L, et al. Time-restricted eating alters the 24-hour profile of adipose tissue transcriptome in men with obesity. Obesity (Silver Spring) 2023;31 Suppl 1:63-74.

[11] Montaigne D, Marechal X, Modine T, Coisne A, Mouton S, Fayad G, et al. Daytime variation of perioperative myocardial injury in cardiac surgery and its prevention by Rev-Erbalpha antagonism: a single-centre propensity-matched cohort study and a randomised study. Lancet 2018;391:59-69.

[12] **Wefers J, van Moorsel D, Hansen J**, Connell NJ, Havekes B, Hoeks J, et al. Circadian misalignment induces fatty acid metabolism gene profiles and compromises insulin sensitivity in human skeletal muscle. Proc Natl Acad Sci U S A 2018;115:7789-7794.

[13] Perrin L, Loizides-Mangold U, Chanon S, Gobet C, Hulo N, Isenegger L, et al. Transcriptomic analyses reveal rhythmic and CLOCK-driven pathways in human skeletal muscle. Elife 2018;7.

[14] van Moorsel D, Hansen J, Havekes B, Scheer FA, Jorgensen JA, Hoeks J, et al. Demonstration of a day-night rhythm in human skeletal muscle oxidative capacity. Mol Metab 2016;5:635-645.

[15] Couto Alves A, Glastonbury CA, El-Sayed Moustafa JS, Small KS. Fasting and time of day independently modulate circadian rhythm relevant gene expression in adipose and skin tissue. BMC Genomics 2018;19:659.

[16] Rinella ME, Lazarus JV, Ratziu V, Francque SM, Sanyal AJ, Kanwal F, et al. A multi-society Delphi consensus statement on new fatty liver disease nomenclature. J Hepatol 2023, doi: 10.1097/HEP.0000000000000520.

[17] Govaere O, Cockell S, Tiniakos D, Queen R, Younes R, Vacca M, et al. Transcriptomic profiling across the nonalcoholic fatty liver disease spectrum reveals gene signatures for steatohepatitis and fibrosis. Sci Transl Med 2020;12:eaba4448.

[18] Vandel J, Dubois-Chevalier J, Gheeraert C, Derudas B, Raverdy V, Thuillier D, et al. Hepatic Molecular Signatures Highlight the Sexual Dimorphism of Nonalcoholic Steatohepatitis (NASH). Hepatology 2021;73:920-936.

[19] **Haas JT, Vonghia L, Mogilenko DA**, Verrijken A, Molendi-Coste O, Fleury S, et al. Transcriptional Network Analysis Implicates Altered Hepatic Immune Function in NASH development and resolution. Nature metabolism 2019;1:604-614.
[20] Lefebvre P, Lalloyer F, Bauge E, Pawlak M, Gheeraert C, Dehondt H, et al. Interspecies NASH disease activity whole-genome profiling identifies a fibrogenic role of PPARalpha-regulated dermatopontin. JCI Insight 2017;2:e92264.
[21] Chen P, Kakan X, Zhang J. Altered circadian rhythm of the clock genes in fibrotic livers induced by carbon tetrachloride. FEBS Lett 2010;584:1597-1601.
[22] Eckel-Mahan KL, Patel VR, de Mateo S, Orozco-Solis R, Ceglia NJ, Sahar S, et al. Reprogramming of the circadian clock by nutritional challenge. Cell 2013;155:1464-1478.
[23] Mure LS, Le HD, Benegiamo G, Chang MW, Rios L, Jillani N, et al. Diurnal transcriptome atlas of a primate across major neural and peripheral tissues. Science 2018;359:eaao0318.
[24] Ruben MD, Wu G, Smith DF, Schmidt RE, Francey LJ, Lee YY, et al. A database of tissue-specific rhythmically expressed human genes has potential applications in circadian medicine. Sci Transl Med 2018;10:eaat8806.
[25] Eckel-Mahan KL, Patel VR, Mohney RP, Vignola KS, Baldi P, Sassone-Corsi P. Coordination of the transcriptome and metabolome by the circadian clock. Proc Natl Acad Sci U S A 2012;109:5541-5546.
[26] Abbondante S, Eckel-Mahan KL, Ceglia NJ, Baldi P, Sassone-Corsi P. Comparative Circadian Metabolomics Reveal Differential Effects of Nutritional Challenge in the Serum and Liver. J Biol Chem 2016;291:2812-2828.
[27] Fujisawa K, Takami T, Matsumoto T, Yamamoto N, Sakaida I. Profiling of the circadian metabolome in thioacetamide-induced liver cirrhosis in mice. Hepatol Commun 2017;1:704-718.
[28] Kettner NM, Voicu H, Finegold MJ, Coarfa C, Sreekumar A, Putluri N, et al. Circadian Homeostasis of Liver Metabolism Suppresses Hepatocarcinogenesis. Cancer Cell 2016;30:909-924.
[29] Malik DM, Paschos GK, Sehgal A, Weljie AM. Circadian and Sleep Metabolomics Across Species. J Mol Biol 2020;432:3578-3610.
[30] Evans AM, DeHaven CD, Barrett T, Mitchell M, Milgram E. Integrated, nontargeted ultrahigh performance liquid chromatography/electrospray ionization tandem mass spectrometry platform for the identification and relative quantification of the small-molecule complement of biological systems. Analytical chemistry 2009;81:6656-6667.
[31] **Tripathi S, Pohl MO**, Zhou Y, Rodriguez-Frandsen A, Wang G, Stein DA, et al. Meta- and Orthogonal Integration of Influenza "OMICs" Data Defines a Role for UBR4 in Virus Budding. Cell Host Microbe 2015;18:723-735.
[32] Zummo FP, Berthier A, Gheeraert C, Vinod M, Bobowski-Gerard M, Molendi-Coste O, et al. A time- and space-resolved nuclear receptor atlas in mouse liver. J Mol Endocrinol 2023;71:e230017.
[33] Pradhan-Sundd T, Vats R, Russell JO, Singh S, Michael AA, Molina L, et al. Dysregulated bile transporters and Impaired tight junctions during chronic liver iInjury in mice. Gastroenterology 2018;155:1218-1232.
[34] **Rydenfelt M, Klinger B,** Klunemann M, Bluthgen N. SPEED2: inferring upstream pathway activity from differential gene expression. Nucleic Acids Res 2020;48:W307-W312.
[35] Lecka-Czernik B, Moerman EJ, Grant DF, Lehmann JM, Manolagas SC, Jilka RL. Divergent effects of selective peroxisome proliferator-activated receptor-gamma 2 ligands on adipocyte versus osteoblast differentiation. Endocrinology 2002;143:2376-2384.
[36] Nagy L, Tontonoz P, Alvarez JG, Chen H, Evans RM. Oxidized LDL regulates macrophage gene expression through ligand activation of PPARgamma. Cell 1998;93:229-240.
[37] Guilliams M, Bonnardel J, Haest B, Vanderborght B, Wagner C, Remmerie A, et al. Spatial proteogenomics reveals distinct and evolutionarily conserved hepatic macrophage niches. Cell 2022;185:379-396.
[38] Klerman EB, Brager A, Carskadon MA, Depner CM, Foster R, Goel N, et al. Keeping an eye on circadian time in clinical research and medicine. Clin Transl Med 2022;12:e1131.
[39] Gentry NW, Ashbrook LH, Fu YH, Ptacek LJ. Human circadian variations. J Clin Invest 2021;131.

637 [40] Yang S, Yamazaki S, Cox KH, Huang YL, Miller EW, Takahashi JS. Coupling-dependent metabolic
638 ultradian rhythms in confluent cells. Proc Natl Acad Sci U S A 2022;119:e2211142119.
639 [41] Oliva-Vilarnau N, Hankeova S, Vorrink SU, Mkrtchian S, Andersson ER, Lauschke VM. Calcium
640 Signaling in Liver Injury and Regeneration. Front Med (Lausanne) 2018;5:192.
641 [42] Arruda AP, Hotamisligil GS. Calcium Homeostasis and Organelle Function in the Pathogenesis
642 of Obesity and Diabetes. Cell Metab 2015;22:381-397.
643 [43] Castelo-Szekely V, Gatfield D. Emerging Roles of Translational Control in Circadian
644 Timekeeping. J Mol Biol 2020;432:3483-3497.
645 [44] Kryuchkova-Mostacci N, Robinson-Rechavi M. A benchmark of gene expression tissue-
646 specificity metrics. Brief Bioinform 2017;18:205-214.

647

Figure legends

Figure 1: Timed liver biopsies from a large cohort of humans with obesity. (A) Overall experimental strategy. (B) Decision tree to stratify the HUL sub-cohort. "HN" (histologically normal), "steatosis" (benign steatosis only) or "MASH" (steatosis+inflammation). (C) Inter-sample variation in gene expression. ANOVA was used to reveal the main sources of overall inter-sample variation. (D) Biopsy daytime distribution. (E) Gene expression analysis. A volcano plot was generated by comparing gene expression using DEseq2 from samples collected in the morning (AM) or in the afternoon (PM) regardless of the pathological state. X axis: $\log_2$ (fold change), Y axis: $-\log_{10}$(p-values). (F) KEGG pathway enrichment analysis. Biological term enrichment was carried out using the 1,660 genes whose expression was significantly different as determined in (E) (FC>1.2, FDR <0.05). (E, F): font size was adjusted for clarity purpose.

Figure 2: A multi-test method identifies time-of-day-dependent genes. *BMAL1/ARNTL* expression as a function of time and of the liver histological grade (A-C). (A) A violin plot is shown to illustrate DEseq2 results to compare AM *vs.* PM expression and correcting for sex as confounding factor. (B) A dot plot with linear tendency lines is shown to illustrate partial Spearman correlation analysis between gene expression and biopsy daytime. (C) A density plot is shown to illustrate the output of the Kolmogorov-Smirnov test for comparison of AM or PM gene expression distributions. (D) Fisher's agglomeration method. Frequency histograms of uncorrected Fisher p-values are shown for each group and the first (colored) bar of each group histogram indicates genes with p<0.05. (E) TDG distribution within histological groups. A Venn diagram shows the unequal distribution of 1,427 TDGs (FC>1.2, FDR<0.01) amongst groups. Numbers indicate the numbers of identified transcripts. (F) Gene expression variation of 132 "common TDGs". CCGs and other transcripts are indicated. * indicates p<0.05 using ANOVA and Fisher's LSD post-hoc test.

Figure 3: Example distributions of time-dependent genes (TDGs) altered in MASH. (A) Violin plots showing AM vs PM gene expression variations for representative TDGs losing their time-dependency in MASH. (B) Violin plots showing AM vs PM gene expression variations for representative TDGs gaining time-dependency in MASH. Statistical tests were Kruskal-Wallis tests followed by unpaired Wilcoxon post-hoc test for AM-PM comparisons in each group (*p<0.05, **p<0.01, ***p<0.005, ****, p<0.001). VST: variance-stabilizing transformation.

Figure 4: Term enrichment analysis of time-dependent genes (TDGs) and upstream regulatory pathway prediction. (A) Biological term enrichment analysis. TDGs identified in Figure 2 were enriched for gene ontology (GO) terms related to biological processes (BP) using Metascape. Significantly enriched GO-BP clusters were manually collapsed for visualization purpose and top hits are indicated. **(B-D):** Pathway activity ranking. Speed2 TDGs enrichment for pathway signature genes. Each pathway is represented as a bar showing the mean rank of the query list. The "bar code" plot shows the distribution of genes from the query list in the ranked reference signatures.

Figure 5: Identification of time-dependent liver metabolites measured by LC-MS. (A) Volcano plot of metabolite time-of-day-dependent differential abundance in liver. Fold-changes values and corresponding p-values obtained using DEseq2 considering sex as confounding factor. (B) Enrichment of KEGG metabolic pathways. A biological term enrichment against the KEGG database was run using the differentially detected metabolites (TDM) identified in (A) (DEseq2 adjusted p-value <0.1). (C) P-value agglomeration by Fisher's method. Similar as gene expression analysis (see Figure 2), p-value agglomeration from three separate statistical tests (DEseq2, partial Spearman correlation, Kolmogorov-Smirnov) was carried out using Fisher's method and identified TDMs within each group. The resulting uncorrected Fisher p-values are shown as frequency histograms and the first (colored) bar of each group histogram indicates metabolites with p<0.1.

Figure 6: Distribution and characterization of time-dependent liver metabolites (TDMs). After correction for multiple testing, 238 metabolites with a Fisher FDR<0.1 were considered

as robustly time-dependent. (A) Distribution of TDMs among liver histological groups. (B-E) KEGG metabolic pathway enrichment of common (central intersection) or group-specific TDMs using the online metabolomics analysis platform MetaboAnalyst.

Figure 7: Integrative analysis of time-dependent genes (TDGs) and metabolites (TDMs). (**A**) Analysis strategy outline. Common and HN- or MASH-specific TDGs and TDMs were analyzed associatively for enrichment of KEGG metabolic pathways using the online metabolomics analysis platform MetaboAnalyst, revealing potential links between metabolic pathways as defined by time-dependent gene expression patterns and metabolomic profiling (**B, C**). Reconstitution (partial) of metabolic pathways displaying time of the day-dependency in the HN (**D**) or MASH (**E**) group. LPA: lysophosphatidic acid, PA: phosphatidic acid, DAG: diacylglycerol, CDP-choline: cytidine-diphosphate-choline, PC: phosphatidylcholine, GPC glycerophosphatidylcholine, X-GPC: acyl-conjugated GPC, 9-HpODE: 9-hydroperoxy octadecadienoic acid, 13-HpODE: 9-hydroperoxy octadecadienoic acid, 9-HODE: 9-Hydroxyoctadecadienoic acid, 13-HODE: 13-Hydroxyoctadecadienoic acid, 12(13)-EpOME: 12(13)-epoxy-9Z-octadecenoic acid, 9,10-EpOME: 9(10)-epoxy-12Z-octadecenoic acid, 12,13-DiHOME: 12,13-dihydroxy-9-octadecenoic acid, 9,10-DiHOME: 9,10-dihydroxy-9-octadecenoic acid.

Table 1: Biometric and biochemical parameters of the HUL sub cohort. The main biometric, biochemical and liver histological features of selected patients are indicated. F: women, M: men; BMI: body mass index; NAS: NAFLD/MASLD Activity Score; HOMA-IR: Homeostatic Model Assessment for Insulin Resistance; AM: ante meridiem, PM: post meridiem. Continuous values are expressed as mean ± SD. Inter-group comparisons were performed using the unpaired Wilcoxon test for continuous variables (age, BMI, HOMA-IR) and Fisher's exact test for the remaining categorical variables.

Figure

Click here to access/download;Figure;Main Fig Johanns_JHepRep_R2.pdf

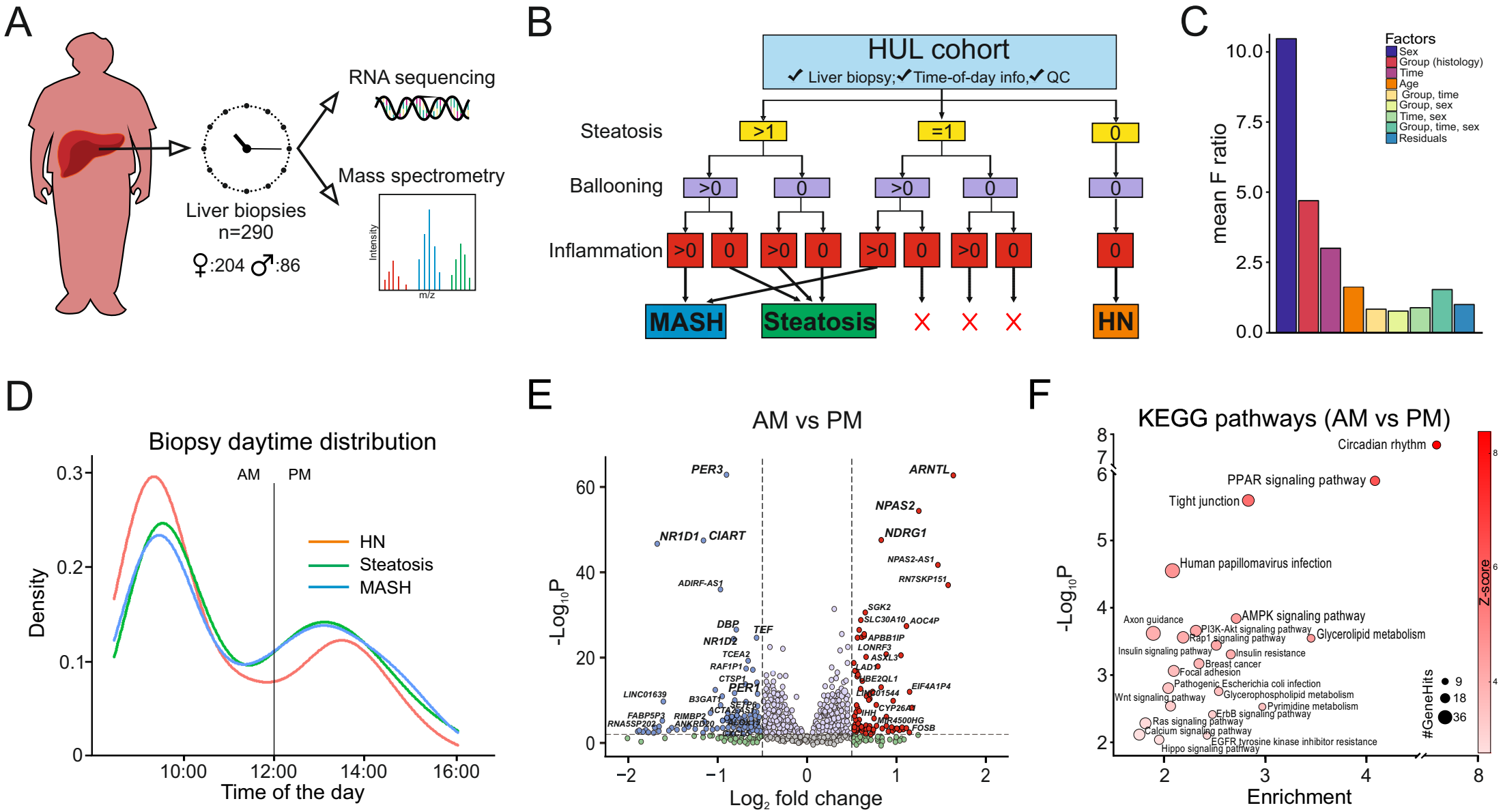

FIGURE 1_R2 - JOHANNS et al.

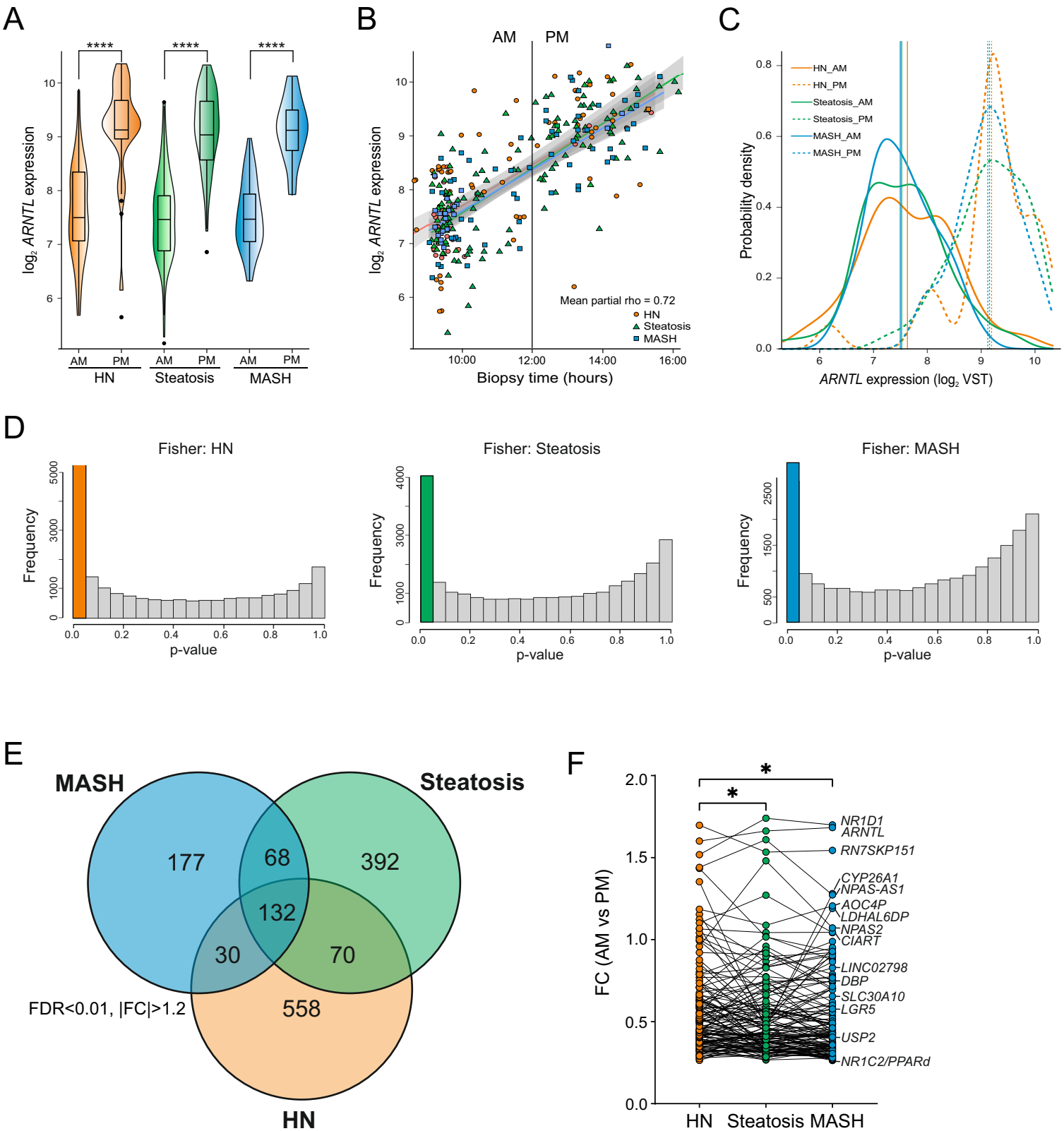

FIGURE 2_R2 - JOHANNS et al.

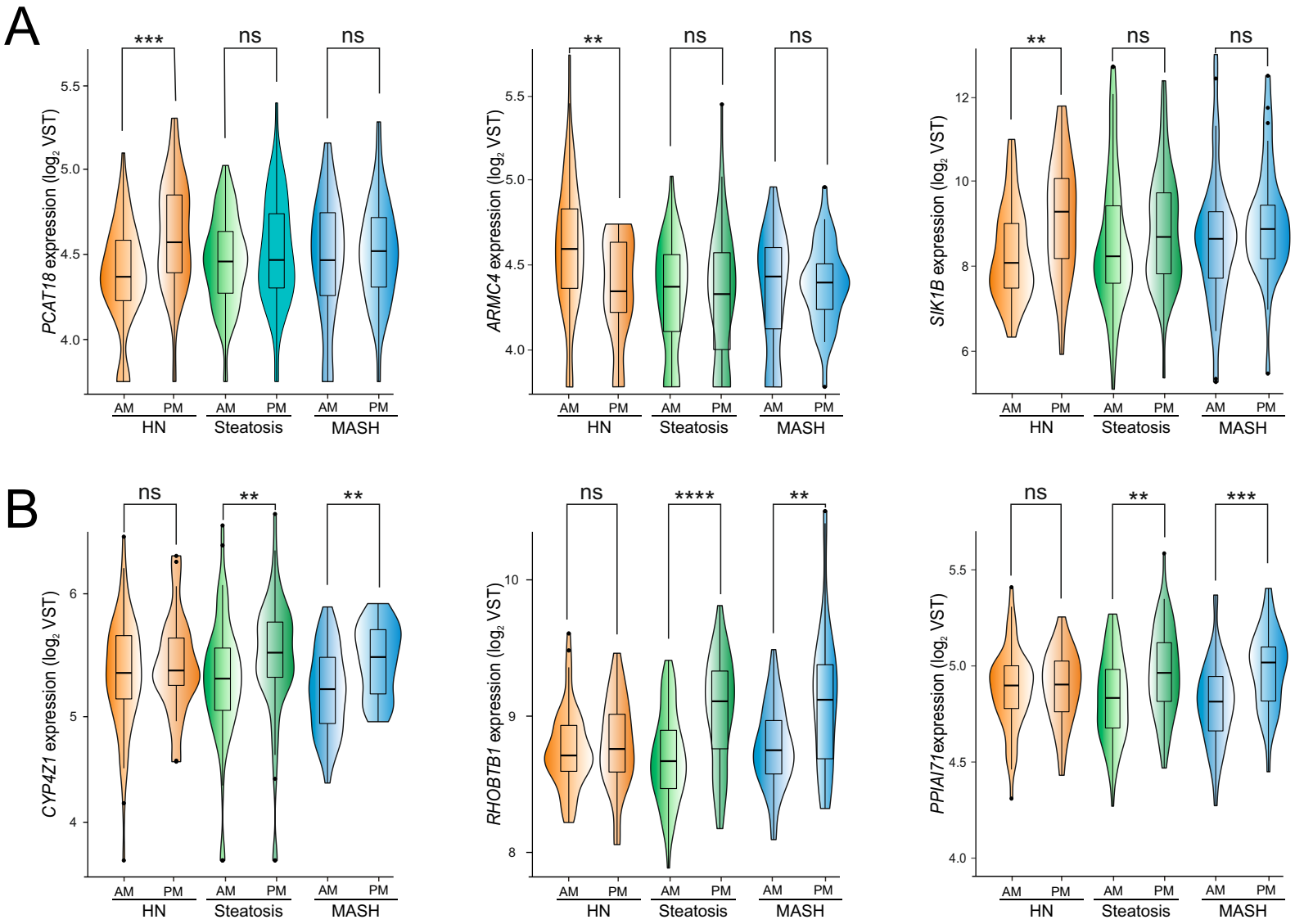

FIGURE 3_R2 - JOHANNS et al.

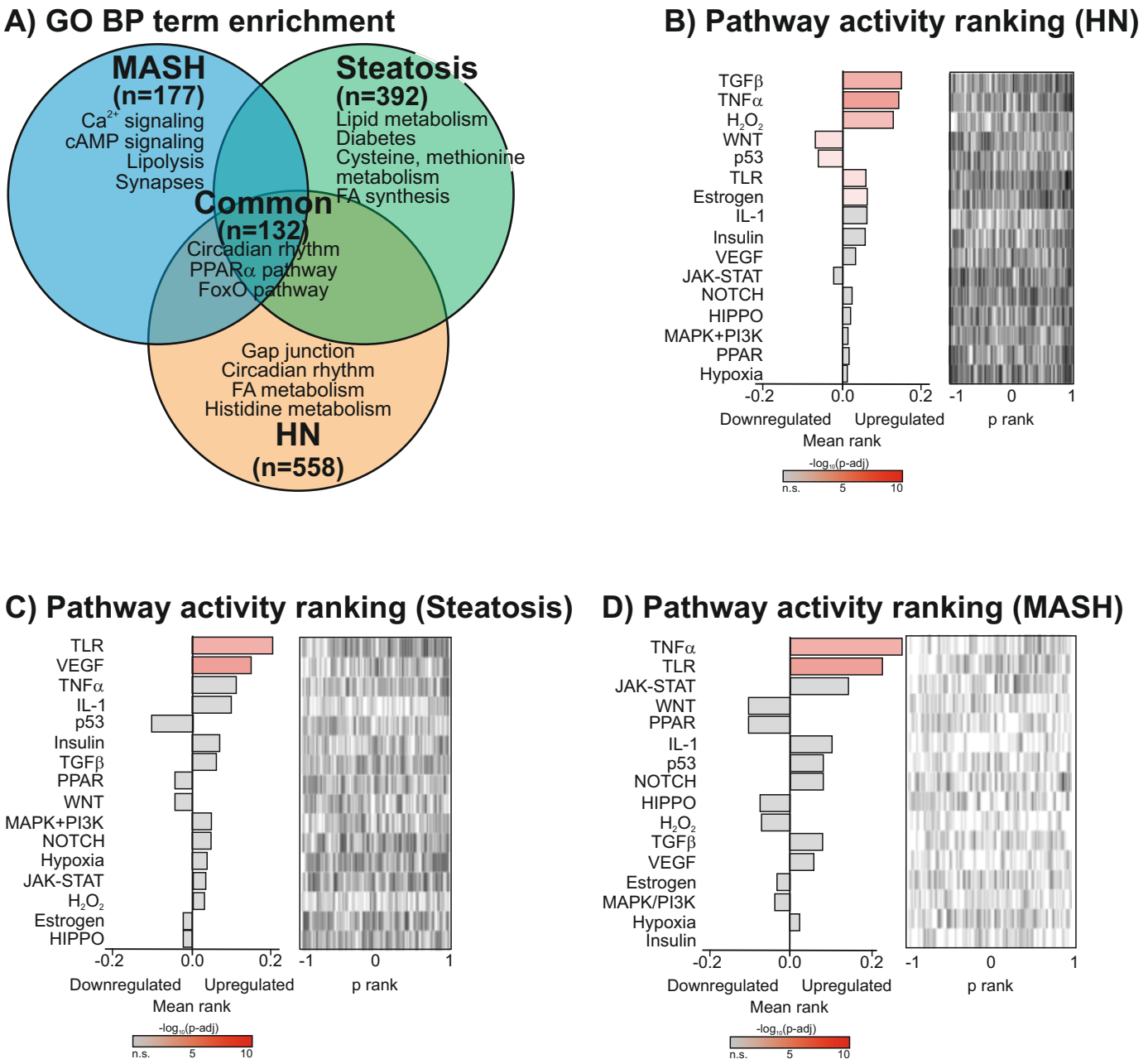

FIGURE 4_R2 - JOHANNS et al.

A

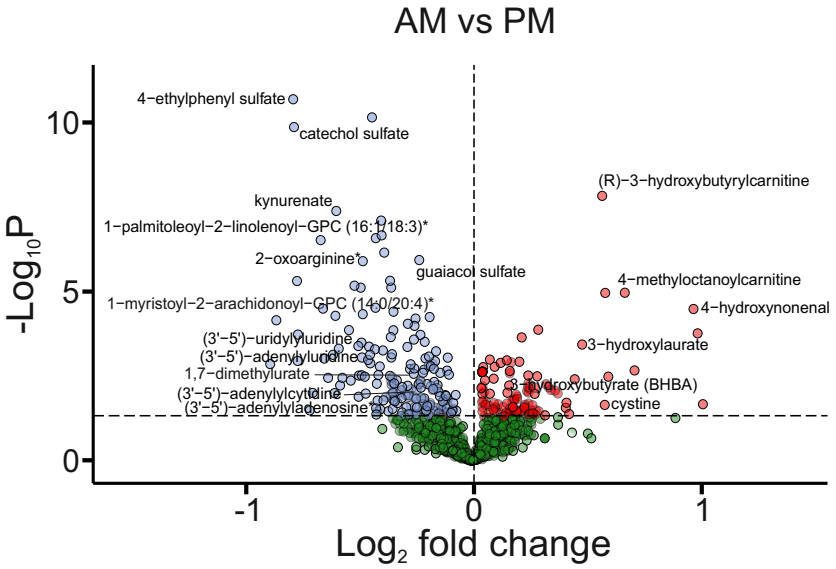

B

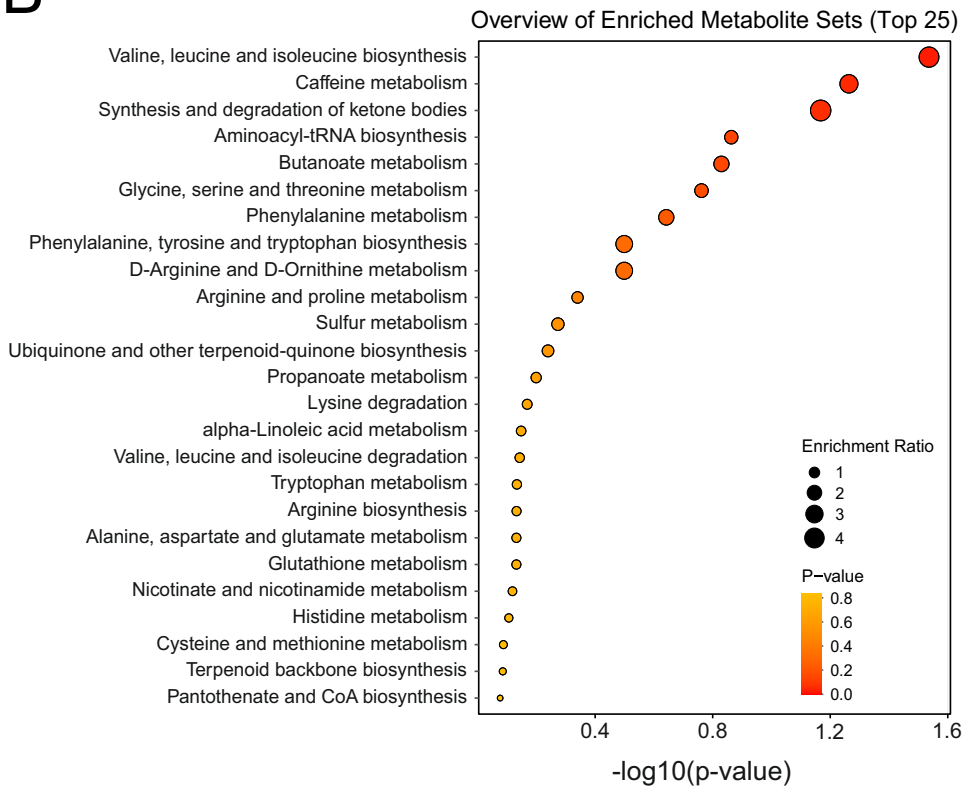

C

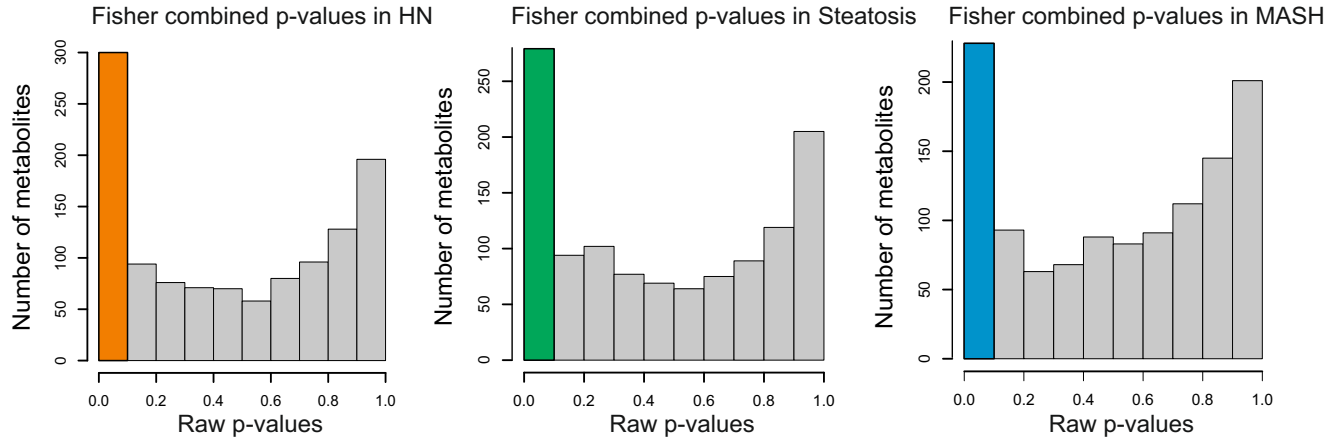

FIGURE 5_R2 - JOHANNS et al.

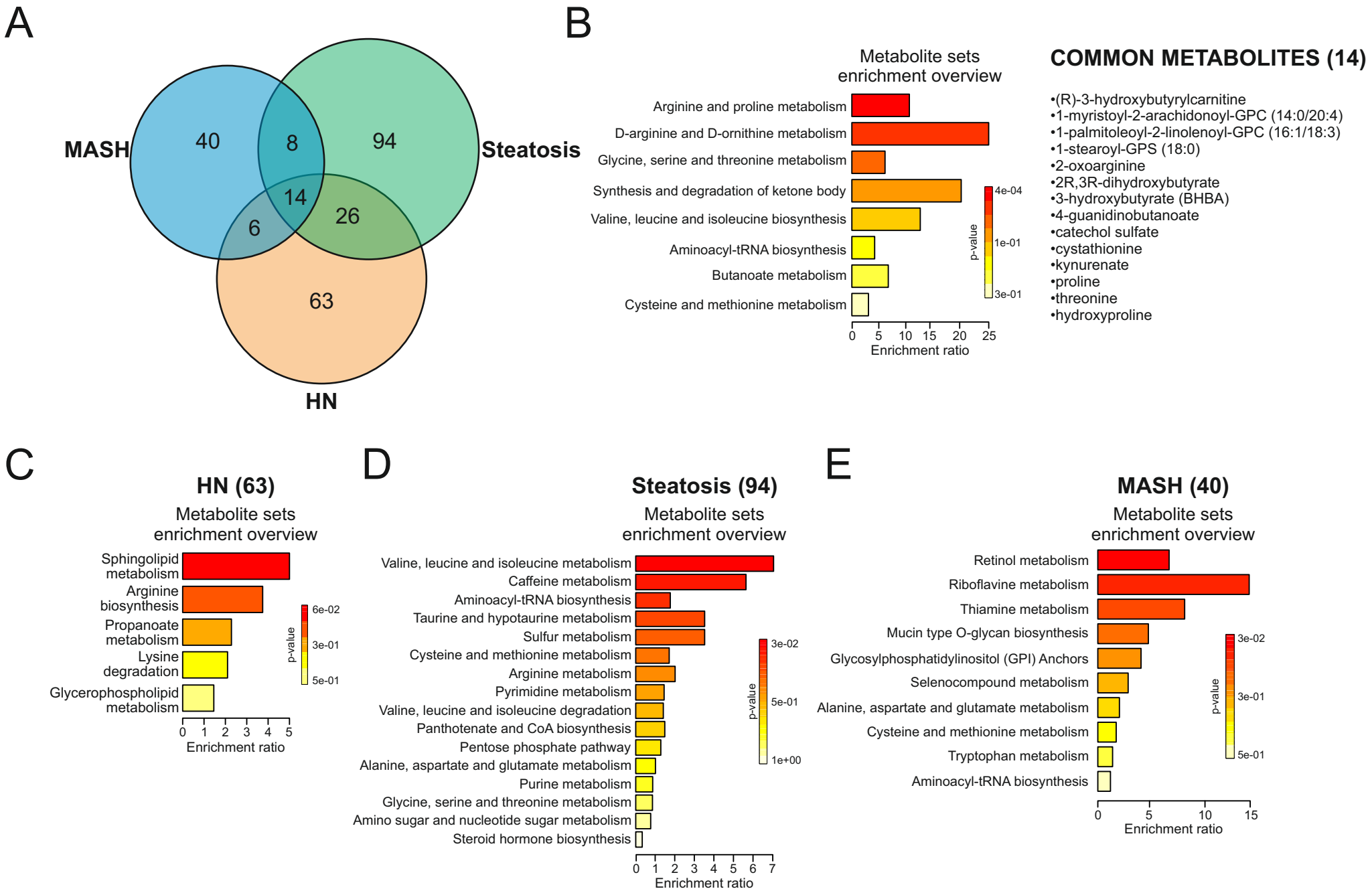

FIGURE 6_R2 - JOHANNS et al.

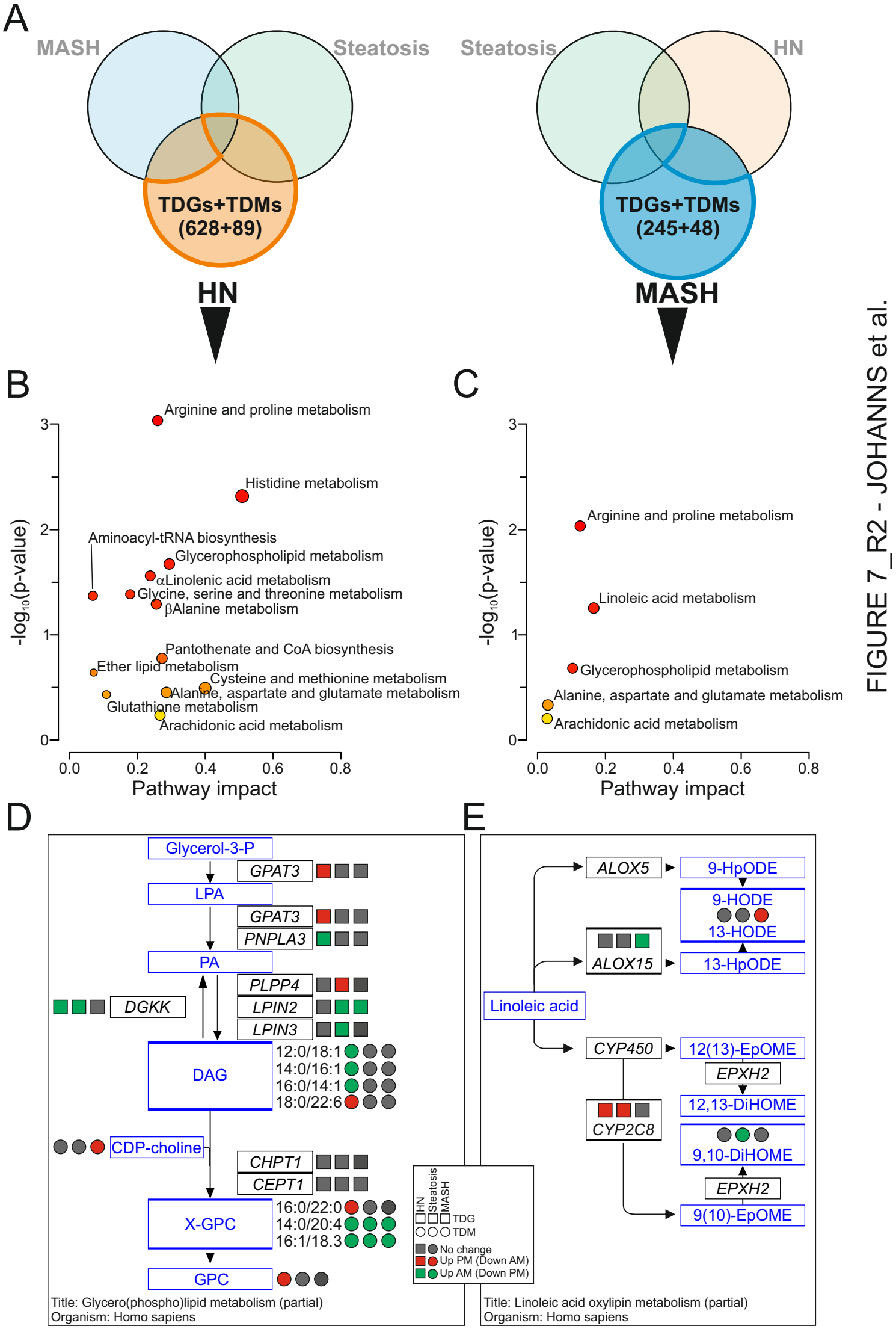

FIGURE 7_R2 - JOHANNS et al.

		MASLD Group			p-values		
Variable	N	**HN**, n = 89	**St.** , n = 122	**MASH**, n = 79	HO *vs.* St.	HO *vs.* MASH	St. *vs.* MASH
Sex	290				0.003	0.008	0.7
F		75/89 (84%)	80/122 (66%)	49/79 (62%)			
M		14/89 (16%)	42/122 (34%)	30/79 (38%)			
Age	290	34.6 ± 11.4	41.8 ± 10.9	46.4 ± 10.4	<0.001	<0.001	0.050
BMI	290	45.4 ± 6.8	47.3 ± 7.9	46.2 ± 7.9	ns	ns	ns
Steatosis score	290				<0.001	<0.001	<0.001
0		89/89 (100%)	0/122 (0%)	0/79 (0%)			
1		0/89 (0%)	0/122 (0%)	18/79 (23%)			
2		0/89 (0%)	71/122 (58%)	29/79 (37%)			
3		0/89 (0%)	51/122 (42%)	32/79 (41%)			
Inflammation score	290				<0.001	<0.001	<0.001
0		89/89 (100%)	70/122 (57%)	0/79 (0%)			
1		0/89 (0%)	44/122 (36%)	55/79 (70%)			
2		0/89 (0%)	8/122 (6.6%)	23/79 (29%)			
3		0/89 (0%)	0/122 (0%)	1/79 (1.3%)			
Ballooning score	290				ns	<0.001	<0.001
0		89/89 (100%)	115/122 (94%)	0/79 (0%)			
1		0/89 (0%)	7/122 (5.7%)	57/79 (72%)			
2		0/89 (0%)	0/122 (0%)	22/79 (28%)			
Fibrosis score (Kleiner)	282				0.009	<0.001	<0.001
0		79/89 (89%)	78/118 (66%)	12/75 (16%)			
1		9/89 (10%)	28/118 (24%)	22/75 (29%)			
2		0/89 (0%)	7/118 (5.9%)	13/75 (17%)			
3		1/89 (1.1%)	5/118 (4.2%)	25/75 (33%)			
4		0/89 (0%)	0/118 (0%)	3/75 (4.0%)			
NAS score	290				<0.001	<0.001	<0.001
0		89/89 (100%)	0/122 (0%)	0/79 (0%)			
2		0/89 (0%)	40/122 (33%)	0/79 (0%)			
3		0/89 (0%)	51/122 (42%)	11/79 (14%)			
4		0/89 (0%)	26/122 (21%)	19/79 (24%)			
5		0/89 (0%)	5/122 (4.1%)	29/79 (37%)			
6		0/89 (0%)	0/122 (0%)	17/79 (22%)			
7		0/89 (0%)	0/122 (0%)	2/79 (2.5%)			
8		0/89 (0%)	0/122 (0%)	1/79 (1.3%)			
HOMA-IR	279	3.8 ± 4.8[1]	13.5 ± 58.8[1]	24.2 ± 55.2[1]	<0.001	<0.001	<0.001
Biopsy time	290				ns	ns	ns
AM		62/89 (70%)	70/122 (57%)	46/79 (58%)			
PM		27/89 (30%)	52/122 (43%)	33/79 (42%)			

TABLE 1_R2 - JOHANNS et al.